Clays and Clay Minerals, Vol. 54, No. 2, 176–194, 2006.

THERMAL AND MINERAL PROPERTIES OF Al-, Cr-, Mn-, Ni- AND Ti-SUBSTITUTED GOETHITE

M. A. WELLS[1,*], R. W. FITZPATRICK[2] AND R. J. GILKES[3]

[1] CSIRO Exploration and Mining, Australian Resources Research Centre (ARRC), PO Box 1130, Bentley, WA 6102, Australia
[2] CSIRO Land and Water, The University of Adelaide, Glen Osmond, Adelaide, SA, 5064, Australia
[3] School of Earth and Geographical Sciences, University of Western Australia, Crawley, WA, 6009, Australia

Abstract—Mineralogical and thermal characteristics of synthetic Al-, Cr-, Mn-, Ni- and Ti-bearing goethites, synthesized via alkaline hydrolysis of metal-ferrihydrite gels, were investigated by powder X-ray diffraction and differential thermal analysis. Shifts in unit-cell dimensions were consistent with size of substituent metal ions and confirmed the incorporation of Al^{3+}, Cr^{3+}, Mn^{3+}, Ni^{2+} and Ti^{4+} in the goethite structure. A weight loss of 6.2 wt.% for goethite containing 12.2 mol.% Ti, being significantly less than for stoichiometric goethite, is consistent with the replacement of Fe by Ti in the goethite structure coupled with the substitution of O^{2-} ions for OH^- (*i.e.* proton loss). These data provide the first confirmation of the direct replacement of Fe by Ti within goethite. Formation of multiple dehydroxylation endotherms for goethite containing 4.5 mol.% Al, 15.3 mol.% Mn and 12.2 mol.% Ti was not attributed to the decomposition of surface OH groups or related simply to the crystallinity of precursor goethite ('high-*a*' *vs*. 'low-*a*') as defined by the magnitude of *a*. Instead, endotherm doublet formation was associated with weight loss due to the dehydroxylation of goethite remaining after initial phase transformation to protohematite and to the evolution of OH^- associated with the rapid increase in crystallite size of protohematite directed primarily along the *a* direction. Development of the first endotherm is due to initial dehydroxylation and transformation to protohematite. With continued heating of well ordered goethite or goethite containing moderate to high levels of substituent cations, domain growth along the *a* direction is delayed or inhibited to a critical point that provides enough thermal energy to enable goethite transformation to proceed to completion and for proto-hematite domain growth to occur. This results in the formation of a second endotherm. For less well ordered goethite and/or goethite containing only low levels of foreign metal cations, protohematite domain growth is not inhibited and proceeds continuously with heating to give only a single endotherm.

Key Words—Dehydroxylation, Differential Thermal Analysis, Double Endotherm, Al-, Cr-, Mn-, Ni- and Ti-substituted Goethite and Hematite, Domain Recrystallization.

INTRODUCTION

The dehydroxylation of goethite to hematite has been the focus of numerous kinetic and structural studies (Naono and Fujiwara, 1980; Watari *et al*., 1983; Wolska and Schwertmann, 1989; Ruan and Gilkes, 1995; Gualtieri and Venturelli, 1999). The dehydroxylation reaction is important commercially in view of its application to the iron ore industry (*e.g.* Weissenborn *et al.*, 1994), and in the production of maghemite for use in audio and video magnetic tapes (Naono and Fujiwara, 1980). The thermal stability of goethite to UV photo-dehydroxylation has also been examined in relation to remote sensing and atmospheric studies of the Martian surface (Morris and Lauer, 1981). Characterization of the goethite to hematite transformation is important in pedological studies, to understand better the processes controlling the formation and distribution of hematite and maghemite, particularly as the temperatures experienced during severe or intense burning can be high enough for goethite dehydroxylation to occur (*e.g.* Anand and Gilkes, 1987).

The transformation of goethite to hematite is topotactic whereby hematite forms via minor modifications of the goethite structure (Bernal *et al.*, 1959). However, recent X-ray diffraction (XRD), infrared (IR) and Raman spectroscopic studies of hematite formed by the dehydroxylation of goethite suggest that the transformation is not as straightforward as previously thought, with the existence of two intermediate, hematite-like phases, 'protohematite' and 'hydrohematite' being proposed (Wolska and Szajda, 1985; Wolska and Schwertmann, 1989; Gualtieri and Venturelli, 1999). Whether these are distinct phases or metastable forms occurring as part of the goethite-to-hematite dehydroxylation continuum remains uncertain. A simplified, schematic representation of the sequence of events and of the products formed during goethite dehydroxylation is presented in Figure 1. This sequence can be further complicated by development of metastable, magnetic, Fe^{2+}-bearing spinels that can form if a transient reducing atmosphere is produced during dehydroxylation or if dehydroxylation occurs in an inert atmosphere (*e.g.* Özdemir and Dunlop, 2000).

* E-mail address of corresponding author:
Martin.Wells@csiro.au
DOI: 10.1346/CCMN.2006.0540204

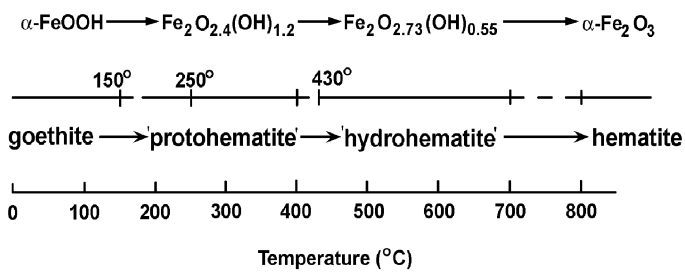

Figure 1. Simplified schematic sequence of the dehydroxylation of goethite to hematite. The terms 'protohematite' and 'hydrohematite' are somewhat controversial and are not yet universally accepted. Distinction of these phases has been made primarily from IR studies where additional bands observed in IR spectra were attributed to the presence of OH^- groups in the hematite structure (Wolska and Szajda, 1985; Wolska and Schwertmann, 1989.

These studies have all mainly dealt with unsubstituted, natural and synthetic goethite with only a few studies reporting on the thermal behavior of Al-substituted goethite (Singh and Gilkes, 1992; Ruan and Gilkes, 1995). Elements other than Al, such as Mn (Stiers and Schwertmann, 1985; Scheinost *et al.*, 2001); Cr (Schwertmann *et al.*, 1989); V (Schwertmann and Pfab, 1994); Co (Gasser *et al.*, 1996), Cd (Huynh *et al.*, 2003) and Ti (Fitzpatrick *et al.* 1978) have also been incorporated into synthetic goethite. Small amounts of transition metals including Ni, Co, Cr, Mn, Cu, Zn, Cd and Pb are also reported to associate with natural and synthetic goethite (Singh and Gilkes, 1992; Trolard *et al.*, 1995; Manceau *et al.*, 2000; Carvalho-de-Silva *et al.*, 2003).

However, the thermal properties of transition metal-substituted goethite have not been well characterized. Previous models to describe the phase transformation of goethite to hematite have been developed primarily from examination of unsubstituted goethite, which may not accurately describe some phenomena observed during dehydroxylation of metal-bearing goethite. For example, the formation mechanism of a 'split' or endotherm doublet for Mn-bearing goethite (Stiers and Schwertmann, 1985) was considered similar to that described for unsubstituted and Al-bearing goethite, which related to the crystallinity of the precursor goethite (Schwertmann, 1984). Unfortunately, Stiers and Schwertmann (1985) did not consider the possible influence of composition (*i.e.* Mn substitution) on endotherm development, which appeared to increase with Mn content.

The aim of this research was to examine the influence that incorporated Al, Cr, Mn, Ni and Ti has on the dehydroxylation properties of synthetic goethite and to describe more fully some of the thermal phenomena recorded during the transformation of goethite to hematite.

METHODS

Pure and Al-, Cr-, Mn-, Ni- and Ti-substituted goethite were prepared from ferrihydrite gels coprecipitated from mixed Fe^{3+}-metal-nitrate solutions by adding excess 6 M KOH to a final pH >13 and ageing of the precipitate at room temperature for 14 days (*e.g.* Schwertmann and Cornell, 1991). The precipitates were mixed by daily shaking of the suspension and ensuring a solution pH >13. Samples were washed with deionized (DI) water to remove excess salts and dried from acetone at 40ºC.

Initial sample characterization

Initial sample treatment entailed removing coprecipitated X-ray amorphous material with two, 60 min acid (pH 3.0) ammonium oxalate extractions in the dark using a sample:solution ratio of 1:200 (Parfitt, 1989), followed by repeated washing with DI water to remove salts and dried from acetone at 40ºC.

Examination by XRD of oxalate-treated samples was performed using a Philips PW 1050 vertical goniometer with 1º receiving and divergence slits, and graphite-diffracted beam monochromator with CuKα radiation. Accurate measurement of *d* values and line-broadening determinations were obtained by step scanning back-filled powder mounts, with 10% NaCl added as an internal standard, at 0.3º2θ/min in 0.01º2θ steps. A crystallographic least-squares template program (Novak and Colville, 1989) was used to calculate the *a*, *b* and *c* unit-cell dimensions of goethite (space group *Pbnm*) for unsmoothed diffraction patterns from the 110, 130, 111 and 140 reflections, corrected for shifts in position and line broadening relative to the NaCl standard. The sizes of coherently diffracting domains (mean crystallite dimension, MCD) were calculated from the Scherrer equation, $MCD_{hkl} = K\lambda/\beta\cos\theta$ (Klug and Alexander, 1974), using a K value of 0.9. Crystallite dimensions along the *a*, *b* and *c* directions of goethite were then calculated by multiplying values of MCD_{hkl} by $\cos\psi$, where ψ is the angle between the vector perpendicular to the *hkl* plane and the unit-cell axis, to enable predictions of crystal shape.

Initial differential thermal analysis (DTA) of oxalate-treated goethite was conducted using a Rigaku TG-DTA Thermoflux 8100 series IR apparatus. Forty-milligram samples were heated in a Pt crucible from ambient to 800ºC at 10ºC/min under N_2 flowing at 40–50 mL/min. Digitized DTA patterns were obtained with a sensitivity

https://doi.org/10.1346/CCMN.2006.0540204 Published online by Cambridge University Press

of 10 μV using Pt-Rh thermocouples and α-Al_2O_3 (corundum) as a base line drift reference material. Samples were prepared by adding small amounts at a time to the Pt crucible and gently tapping the crucible on the bench to pack the sample and obtain a level surface. Samples were compressed using a stainless steel plunger (mass 51.81 g, diameter 4.5 mm) to a pressure of ~3.2×10^4 N/m^2. This procedure was repeated until the desired mass (*i.e.* 40 mg) was obtained. A ventilated Pt lid of diameter 4.5 mm placed on top of the sample prevented loss of material during heating. Sample preparation and packing conditions are classified as 'soft' (Mackenzie and Berggren, 1970).

Surface areas of oxalate-treated goethite were obtained using the BET N_2 single point adsorption method with a p/p_O value of 0.18. Transmission electron microscopy (TEM) of unheated goethite was performed using a Philips 430 analytical transmission electron microscope (ATEM) operating at 300 kV. For examination by TEM, samples were prepared by air drying suspensions on carbon-coated copper grids.

Goethite with multiple DTA endotherms

Goethite with multiple endotherms, recorded during initial DTA examination, were re-examined using DTA and XRD analysis to determine the nature of the endotherm doublet. As initial treatment involved extraction with ammonium oxalate, decomposition of surface oxalate complexes during heating may have complicated the dehydroxylation behavior recorded. Ammonium oxalate is readily adsorbed onto the goethite surface through ligand exchange via formation of mononuclear and bidentate complexes that replace OH groups (Parfitt *et al.*, 1977; Suter *et al.*, 1991). During heating, decomposition of surface-absorbed oxalate complexes would contribute to the overall weight loss recorded and complicate (*e.g.* broaden) the DTA pattern recorded during goethite dehydroxylation (Huynh *et al.*, 2003). Consequently, relating features of the endotherm to effects only associated with the dehydroxylation of goethite would be difficult.

In view of the potential problems associated with using ammonium oxalate, samples of freshly prepared material, selected for re-examination, were treated with 0.4 M HCl to remove associated X-ray amorphous and poorly-ordered material following the method of Cornell and Schneider (1989), dialyzed against DI water until the electrical conductivity was equivalent to that for DI water (~1.0 μS cm^{-1}), before drying at 50°C. Simultaneous DTA patterns and weight-loss determinations were obtained using a TA Instruments SDT 2960 thermal analyzer by heating ~40 mg unpacked samples in a Pt crucible from room temperature to 500ºC at 10°C/min under a N_2 atmosphere flowing at 100 cm^3 min^{-1}. The comparatively large sample sizes of ~40 mg were used in the present study to: (1) provide enough material for sequential XRD analysis, (2) enable a comparison with previous studies where similar phenomena have been reported for samples of similar weight (*e.g.* 50 mg) (Stiers and Schwertmann, 1985), and (3) enhance effects associated with the dehydroxylation of bulk goethite samples.

From the initial DTA patterns recorded for the bulk, HCl-treated samples, points were selected that corresponded to particular features of the DTA endotherm for each sample (Figure 4). Separate, individual 40 mg subsamples of HCl-treated goethite were, in each case, heated under the same instrumental conditions as previously described, to the temperatures selected before stopping the instrument and allowing the sample to cool to room temperature. Being a water-cooled instrument, this procedure took <1 min after interruption of the heating sequence. A composite plot of raw DTA data recorded for each individually heated 40 mg sub-sample of, in this case, Al-bearing goethite, heated using the procedure described is shown in Figure 4e. The DTA patterns recorded for the HCl-treated, Al-bearing goethite demonstrate the reproducible nature of the thermal behavior recorded. The same consistent thermal behavior was observed for the remaining HCl-treated goethites (data not shown) and demonstrates the homogeneous nature of the synthetic goethites examined in this study.

These 'partially dehydroxylated' samples were then prepared for XRD analysis by adding either 20% of 1 μm sized ZnO (zincite), or 20% of 10 μm sized α-Al_2O_3 (corundum), as an internal standard and gently grinding the mixture under ethanol to obtain an homogeneous mixture. Each mixture was fixed to a glass slide with ethanol and air dried before XRD analysis. A crystallographic least-squares template program (Novak and Colville, 1989) was used to calculate unit-cell dimensions of partially dehydroxylated goethite using *d* values for the 020, 110, 120, 130, 111, 140, 211, 221, 160, 250 and 061 reflections of goethite, and the 012, 104, 110, 113, 116 and 300 reflections of hematite formed from goethite after correction for line broadening and instrumental shifts, relative to either ZnO or α-Al_2O_3. We could not ascertain any systematic errors in the XRD analysis of goethite and hematite as a consequence of the different methods used in the preparation (*i.e.* random powder *vs.* glass mounts) of samples for XRD analysis.

RESULTS AND DISCUSSION

XRD analysis (pre-treatment with ammonium oxalate)

The XRD analysis confirmed, to within the detection limit (*i.e.* ~2–5 wt.%), that samples consisted entirely of monomineralic goethite. Whilst use of ammonium oxalate would influence the thermal behavior of goethite, its use to initially 'clean' and prepare samples for XRD analysis would not have affected the bulk structure of goethite and hence, have had no influence on

https://doi.org/10.1346/CCMN.2006.0540204 Published online by Cambridge University Press

unit-cell values. In the following discussion, values of *a*, *b* and *c* unit-cell dimensions averaged for the three control goethites were used to investigate the relationship between unit-cell size and metal-substitution unless otherwise stated.

Unit-cell *b* and *c* dimensions of Al-substituted goethite decreased ($b = 9.941 - 7.16 \times 10^{-3}$ mol.% Al; $r^2 = 0.80$**; $c = 3.020 - 2.27 \times 10^{-3}$ mol.% Al; $r^2 = 0.82$**, where ** represents a 95% confidence limit), with incorporation of Al (Table 1). Shifts in the unit-cell dimensions, towards those of the isostructural end-member diaspore, α-AlO.OH, are consistent with the replacement of Fe^{3+} in goethite by the smaller Al^{3+} ion (Table 2) (Schulze and Schwertmann, 1984). Unit-cell *a* values for Cr-bearing goethite systematically decreased with Cr substitution ($a = -3 \times 10^{-4}$ mol.% Cr + 0.46; $r^2 = 0.92$***, where *** represents a 99% confidence limit), and were significantly different to the range in *a* observed for the control goethites. Whilst values of *b* also showed a systematic decrease with Cr content when compared to the mean *b* value for the control samples, overall changes in *b* for Cr-bearing goethite are within the range in *b* identified for the three controls (Table 1). Changes in the *c* unit-cell dimension for Cr-bearing goethite were unrelated to Cr substitution (Table 1). Unit-cell dimensions of Cr-substituted goethite produced under similar conditions of high pH were reported to be linearly related to Cr contents up to 12 mol.%, with *c* showing a closer relationship to Cr substitution than either *a* or *b* (Schwertmann *et al.*, 1989). The greater range in Cr content of the goethites examined by Schwertmann *et al.* (1989) may have allowed a better identification of the relationships between unit-cell dimensions and Cr content compared to samples examined in this study.

Incorporation of Mn within the goethite structure resulted in contraction of the goethite unit-cell along the *a* and *c* directions (Table 1), and an increase along the *b*

Table 1. Mineralogical properties of oxalate-treated pure and metal-substituted goethite (Space group *Pbnm*).

Nominal mol.%	Measured mol.%[1]	Unit-cell dimensions (nm)[2]			MCD (nm)[4]			SA[5]
		a	*b*	*c*	MCD*a*	MCD*b*	MCD*c*	($m^2\ g^{-1}$)
C1	0	0.4637(2)	0.9941(2)	0.3021(1)	8.5(0.7)	31.8	>12.3	60
C2	0	0.4643(2)	0.9940(2)	0.3016(1)	7.9(0.7)	24.5	>11.2	63
C3	0	0.4623(1)	0.9955(1)	0.3025(0)	8.1(0.8)	31.7	>11.1	66
(Mean)		0.4634	0.9945	0.3021				
Al; 5	2.1	0.4635(0)	0.9921(0)	0.3012(0)	10.9(0.5)	41.6	>16.5	63
10	3.0	0.4609(0)	0.9930(0)	0.3015(0)	12.9(1.6)	38.3	>20.2	50
15	3.8	0.4632(1)	0.9910(1)	0.3011(0)	15.7(1.2)	56.0	>23.9	51
20	4.6	0.4617(0)	0.9913(0)	0.3010(0)	16.6(1.2)	37.5	>26.2	39
Cr; 1	0.9	0.4638(2)	0.9942(2)	0.3018(1)	10.0(0.7)	39.7	>14.4	64
3	2.8	0.4626(1)	0.9942(1)	0.3017(0)	10.1(1.0)	35.7	>14.4	63
5	4.7	0.4625(1)	0.9948(0)	0.3019(0)	10.4(0.9)	32.6	>15.7	60
10	8.7	0.4612(0)	0.9951(0)	0.3019(0)	11.9(1.3)	50.0	>16.9	55
Mn; 4	3.5	0.4616(2)	0.9947(2)	0.3015(1)	8.2(1.0)	30.8	>12.2	69
8	7.2	0.4621(1)	0.9956(1)	0.3014(0)	8.4(1.2)	28.1	>13.0	90
12	10.8	0.4606(2)	0.9986(2)	0.3004(1)	10.2(1.3)	25.7	>14.9	73
16	15.3	0.4608(1)	0.9985(1)	0.3006(0)	9.9(1.6)	25.3	>13.9	60
Ni: 3	2.7	0.4641(1)	0.9948(1)	0.3018(0)	10.1(1.4)	27.5	>13.6	59
5	3.9	0.4624(3)	0.9967(3)	0.3023(1)	9.8(0.9)	33.2	>14.1	61
7	4.5	0.4631(3)	0.9969(3)	0.3022(1)	10.1(1.7)	26.5	>14.6	56
15	5.0	0.4632(1)	0.9972(1)	0.3023(0)	12.0(2.2)	32.4	>16.6	55
Ti; 5	4.1	0.4629(2)	0.9945(1)	0.3020(1)	9.4(1.1)	33.6	>13.8	47
10	6.8	0.4621(2)	0.9945(2)	0.3019(1)	11.3(1.6)	34.3	>14.0	51
15	12.2	0.4629(1)	0.9940(1)	0.3015(0)	15.8(5.1)	34.6	>16.2	88

[1] mol.% metal = [metal/(metal + Fe)] × 100%, determined after complete dissolution of 50 mg samples in 30 mL of conc. HCl and analysis for Fe and metal by AAS.
[2] Values in parentheses represent the standard deviation of unit-cell values.
[3] Weight loss determined as the average of duplicates for the interval 105–700ºC.
[4] Mean crystallite dimensions (MCD) along the goethite unit-cell *a*, *b* and *c* directions. MCD_{020} was taken as a direct measure of crystallite size along the *b* direction. MCD_c was calculated from MCD_{111} and is a minimum value (Schulze and Schwertmann, 1987). Values in parentheses are the standard deviation for MCD values along the *a* direction.
[5] Specific surface area (SA) determined by BET-N_2 adsorption.

https://doi.org/10.1346/CCMN.2006.0540204 Published online by Cambridge University Press

direction (b = 9.941 + 3.12×10^{-3} mol.% Mn; r^2 = 0.85**). This is consistent with incorporation of Mn^{3+} into the goethite structure, even though Fe^{3+} and Mn^{3+} have similar ionic size (Table 2), causing Mn-O/OH octahedra to become distorted (*i.e.* Jahn-Teller effect), with unit-cell dimensions shifting towards the Mn end-member groutite, α-MnOOH (Stiers and Schwertmann, 1985; Scheinost *et al.*, 2001). Apical Mn−O bonds lengthen relative to equatorial Mn−O/OH bond lengths, which are directed along the b direction in goethite (Scheinost *et al.*, 2001). The major increase along the b direction accounts for the overall increase in unit-cell volume (Table 1).

Unit-cell a and c dimensions of Ni-bearing goethite were not significantly different from those for control goethites (Table 1). However, the b dimension was linearly related (b = 9.942 + 5.77×10^{-3} mol.% Ni; r^2 = 0.83**) with increasing Ni content to ~5.0 mol.%. This is consistent with incorporation of the larger Ni^{2+} ion relative to Fe^{3+} (Table 2) and is in agreement with reports of the goethite unit-cell expanding along the b direction with incorporation of Ni to ~6 mol.% (Cornell *et al.*, 1992; Manceau *et al.*, 2000; Carvalho-de-Silva *et al.*, 2003). Manceau *et al.* (2000) and Carvalho-de-Silva *et al.* (2003) recently confirmed the incorporation of Ni^{2+} within the structure of goethite using extended X-ray absorption spectroscopy (XAS). Incorporation of Ni in the goethite structure may involve the coupled substitution of Ni^{2+} with H^+ for Fe^{3+} to maintain charge neutrality, converting $FeO_3(OH)_3$ octahedra into $NiO_2(OH)_4$ (Carvalho-de-Silva *et al.*, 2003) This coupled substitution is accommodated by local dilation of the goethite structure (Carvalho-de-Silva *et al.*, 2003) manifested as an expansion of the unit-cell along the b direction, which accounts for the overall increase in unit-cell volume with increasing Ni content (Table 1).

Unit-cell a and b dimensions for goethite containing Ti were not related to increasing amounts of Ti, and the changes in a and b observed were within the range for a and b of the control samples (Table 1). However, the c dimension (c = 3.022−4.97×10^{-4} mol.% Ti; r^2 = 0.93***) and unit-cell volume (V = 139.18−0.043 mol.% Ti; r^2 = 0.83**) of Ti-bearing goethite were negatively related to Ti content. This is consistent with Fe^{3+} being replaced by the slightly smaller Ti^{4+} ion (Table 2). Previous attempts to produce goethite containing Ti have reported only minor, non-systematic shifts in the d spacings of reflections (Fitzpatrick *et al.*, 1978; Vempati *et al.*, 1991). Reported associations of Ti with natural goethite were not reflected in shifts in the position of diffraction lines (Trolard *et al.*, 1995), with replacement of Fe^{3+} by Ti^{4+} within natural Fe oxides being inferred from the charge characteristics of tropical soils (Tessens and Zauyah, 1982) or from selective dissolution data in podzols (Fitzpatrick and Chittleborough, 2002). We reason that incorporation of Ti^{4+} may be facilitated by O^{2-} replacing OH^- ions in the goethite structure (*i.e.* effectively the loss of a proton). Alternatively, substitution of Ti^{4+} may involve the replacement of $4Fe^{3+}$ by $3Ti^{4+}$ ions to maintain charge neutrality. This would produce a cation-deficient or defect structure, which, if vacancies were regularly distributed throughout the structure, may show in XRD patterns as a superstructure similar to that for maghemite (van Oosterhaut and Rooijmans, 1958). However, no superstructure lines were observed in XRD patterns for Ti-bearing goethite, which suggests the occurrence of a random cation-defect structure with substitution of Ti^{4+} coupled with O^{2-} replacing OH^- ions. Further study using XAS is required to understand fully the nature of Ti incorporation within goethite.

Goethite morphology: TEM examination (ammonium-oxalate treated)

Selected area electron diffraction (SAED) analysis of the typical lath-shaped crystals of most of the goethites examined indicated that the a direction was parallel to the electron beam and that crystal particles were elongated along the c axis (Cornell *et al.*, 1983).

Most goethites from this study examined by TEM show a uniform, well-developed lath morphology with stepped crystal terminations (Figure 2). This habit is typical of goethites prepared at high pH (*e.g.* Schulze and Schwertmann, 1987). Crystals are probably domi-

Table 2. Stereochemistry of metal ions in octahedral coordination.

Ion	Metal-oxygen bond energy (kJ/mole)[1]	Ionic radius[2] (nm)	Octahedral CFSE[3] (kJ/mole)[1]	Site preference energy[3] (kJ/mole)[1]
Al^{3+}	29.3	0.0535	–	–
Cr^{3+}	24.5	0.0615	14.2	46.7
Fe^{3+}	23.7	0.0645	0	0
Mn^{3+}	23.0	0.0645	8.60	25.3
Ni^{2+}	21.8	0.0690	7.07	22.5
Ti^{4+}	38.4	0.0605	0	0

[1] *Handbook of Chemistry and Physics* (1988). Bond energies are for a standard temperature of 298 K.
[2] Shannon (1976)
[3] Crystal field stabilization energy, Burns (1970)

https://doi.org/10.1346/CCMN.2006.0540204 Published online by Cambridge University Press

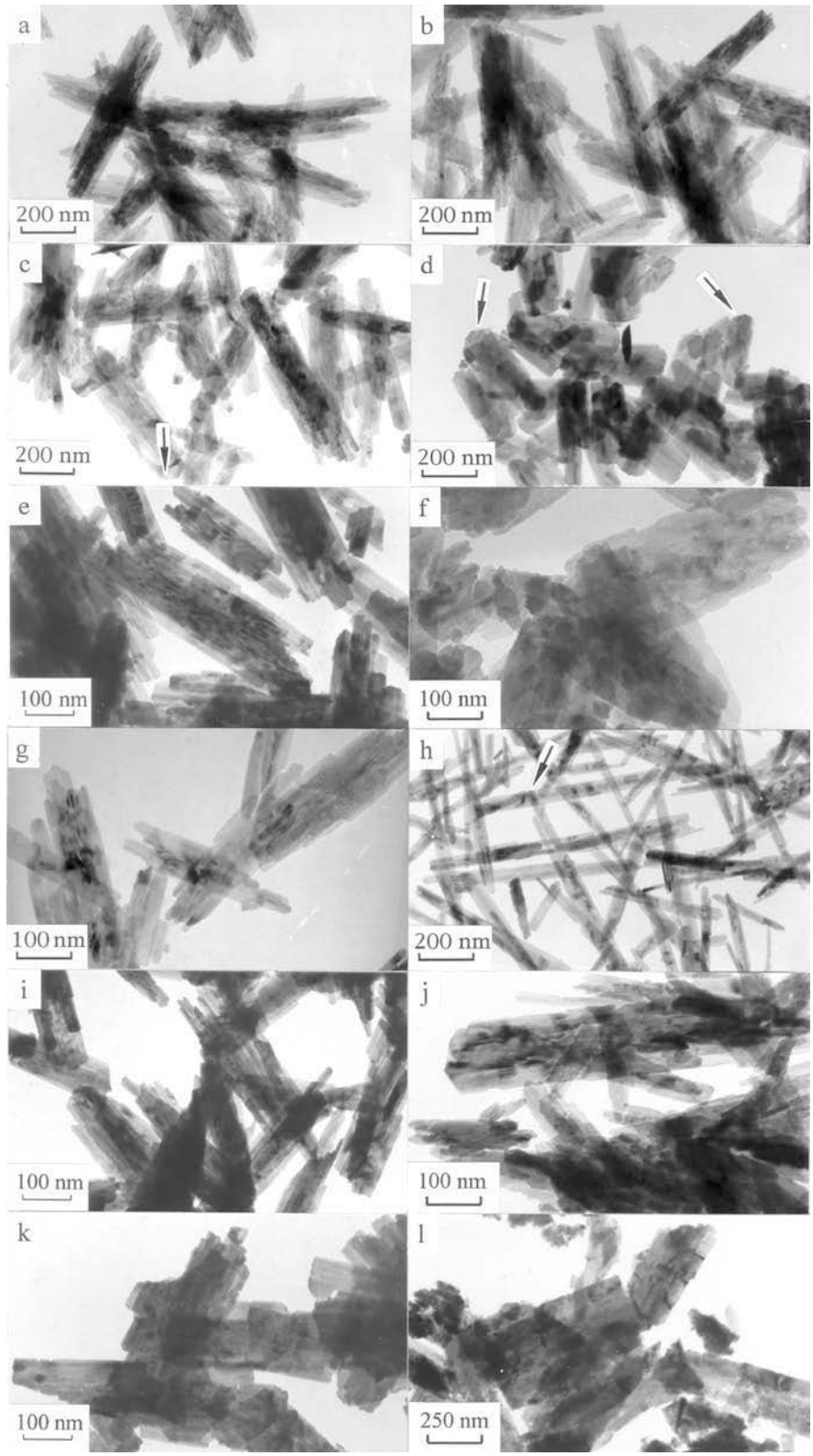

Figure 2. TEM images of unheated (a,b) control; (c) 2.1 mol.% Al; (d) 4.6 mol.% Al; (e) 0.9 mol.% Cr; (f) 8.7 mol.% Cr; (g) 3.1 mol.% Mn; (h) 15.3 mol.% Mn; (i) 2.7 mol.% Ni; (j) 5.0 mol.% Ni; (k) 4.1 mol.% Ti and (l) 12.2 mol.% Ti goethite. Goethite crystals are often terminated by well developed (021) faces, in particular Al- and Mn-bearing goethites (arrowed).

https://doi.org/10.1346/CCMN.2006.0540204 Published online by Cambridge University Press

nated by (010) and (001) faces, although high-resolution TEM studies of natural and synthetic goethite sectioned normal to (001) have reported that (110) faces may dominate giving goethite crystals diamond-shaped cross-section (Smith and Eggleton, 1983).

Goethite with 2.1 mol.% Al, 3.5 mol.% Mn and 2.7 mol.% Ni have a lath-like morphology similar to the unsubstituted control samples, with crystals often showing stepped terminations (Figure 2c,i). Goethite containing Ti and, to a lesser extent, Cr, has a more prismatic or blocky habit (Figure 2k,l and e,f).

Incorporation of Ni had little effect on the morphology or size of goethite particles (Table 3), with crystals retaining a raft-like morphology over the range of Ni substitution (2.7–5.0 mol.%) studied (Figure 2i,j). Goethites containing the maximum amount of Al (4.6 mol.%) and Mn (15.3 mol.%) consist of well developed, euhedral crystals often terminating with 021 faces (Figures 2d and h, respectively). Incorporation of 4.6 mol.% Al retarded growth along the *c* direction (Table 3), which is consistent with several reported observations on goethite with similar Al contents synthesized under similar conditions (*e.g.* Schulze and Schwertmann, 1987). Incorporation of Mn to ~15 mol.% resulted in a contraction along the *b* direction (*i.e.* width) and a lengthening along the *c* direction (*i.e.* length) (Table 3) to produce acicular crystals (Figure 2h). A similar acicular morphology was reported for Mn-bearing goethites produced under similar conditions of high pH by Stiers and Schwertmann (1985). Structural strain associated with the incorporation of octahedrally distorted Mn^{3+} may have inhibited lateral development of double chains of Fe/Mn-octahedra that run normal to the *b* direction by weakening the H bonds that link the double chains, resulting in the needle-like forms.

Initial thermal analysis (pre-treatment with ammonium oxalate)

As discussed previously, pretreatment using ammonium oxalate is problematic because the decomposition of surface-adsorbed oxalate species during heating would contribute to the weight loss recorded during goethite dehydroxylation. Consequently, no examination pertaining to weight loss is made in the following section. However, because all samples were treated under identical conditions, an evaluation can be made of the relative influence that foreign cations may have on dehydroxylation temperature within a series of metal-bearing goethite, assuming a similar adsorption mechanism for oxalate at the surface of goethite particles of a similar morphology (*e.g.* Al-, Cr- and Ni-bearing goethites).

The DTA patterns for Mn-, Ni- and Ti-substituted goethites show a broad endotherm at 20–100ºC (Figure 3). This is consistent with reported observations for synthetic goethite and was attributed to surface-water desorption (Mackenzie and Berggren, 1970; Derie *et al.*, 1976; Schwertmann *et al.*, 1985). However, in this case, the decomposition of surface-coordinated oxalate-groups may also have contributed to the weight loss recorded over this temperature range.

Table 3. Crystal size of control and metal-substituted goethite from TEM observations.

Sample	Mol.%	Width (nm)[1]	Length (nm)[1]	D[2]	n
C1	0	131(15)	606(91)	4.1	7
C2	0	139(17)	584(91)	5.7	8
C3	0	112(25)	637(110)	3.5	11
	Av = 127	Av = 609			
Al	2.1	145(18)	586(52)	3.5	28
	4.6	133(25)	417(73)	3.5	9
Cr	0.9	463(19)	590(52)	11.7	20
	8.7	186(31)	442(49)	3.7	9
Mn	3.5	95(13)	376(29)	3.1	12
	15.3	47(13)	560(178)	1.9	20
Ni	2.7	112(15)	547(62)	4.1	22
	5.0	110(41)	540(202)	3.4	3
Ti	4.1	244(53)	676(114)	7.3	9
	12.2	332(73)	808(228)	9.6	8

[1] Standard deviation of width and length determinations given in parentheses.
[2] D is the number of crystallites or domains along the width of each goethite crystal. Values of D were calculated by dividing the goethite crystal width (from TEM observations) by the value of domain size along the goethite *b* direction (*i.e.* MCD*b*).
n = number of observations.

https://doi.org/10.1346/CCMN.2006.0540204 Published online by Cambridge University Press

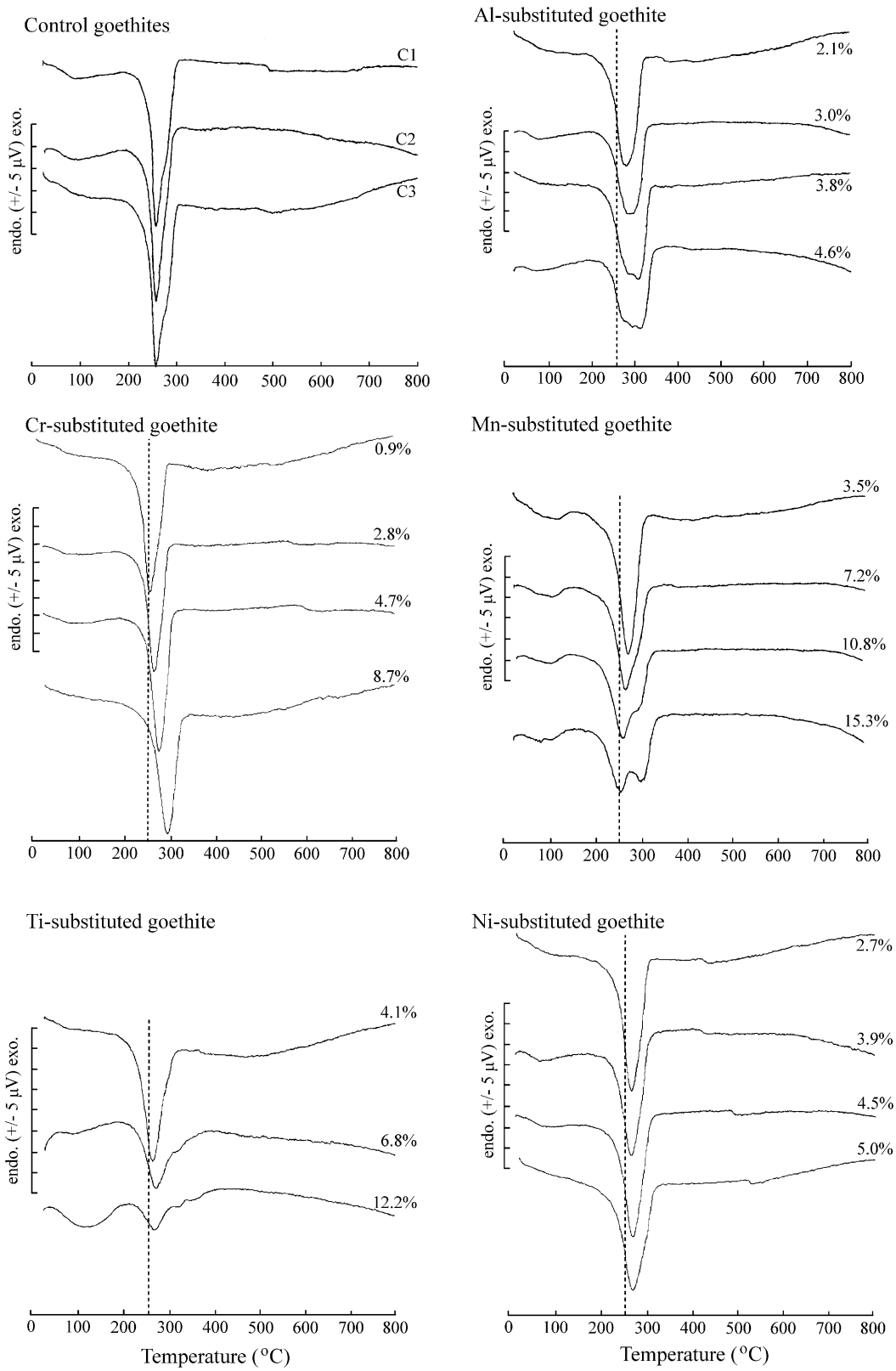

Figure 3. DTA patterns of oxalate-treated control and metal-substituted goethites. The dotted vertical line in the DTA patterns for metal-bearing goethites represents the averaged endotherm temperature (*i.e.* 256°C) for the three control goethites.

https://doi.org/10.1346/CCMN.2006.0540204 Published online by Cambridge University Press

Dehydroxylation of all goethites was generally characterized by a single endotherm between 250 and 300ºC (Figure 3). Endotherm temperatures of Al-substituted goethites generally increased with incorporation of Al, consistent with published data (Singh and Gilkes, 1992). Endotherm temperatures for Cr-bearing goethites were positively related to Cr content (T = 255 + 5.032 mol.% Cr; r^2 = 0.99***).

These increases in dehydroxylation temperature for Al- and Cr-substituted goethite can be explained by the greater metal−O/OH bond energy for Al^{3+} and Cr^{3+}, relative to Fe^{3+} (Table 2). Incorporation of Al and Cr increased the thermal stability of goethite, delaying its transformation to hematite to a higher temperature. Dehydroxylation temperatures increased towards the values for the isostructural Al- and Cr-analogues, diaspore (α-AlOOH) and bracewellite (α-CrOOH). Diaspore and bracewellite transform topotactically to their respective oxides, α-Al_2O_3 at 540−580ºC (Hsu, 1989), and Cr_2O_3 at 440−460ºC (Mackenzie and Berggren, 1970), whereas Fe_2O_3 forms at 250−400ºC (Schwertmann and Taylor, 1989). The higher dehydroxylation temperature of α-AlOOH relates to the greater Al−O/OH bond energy relative to that for Cr or Fe (Table 2).

The DTA patterns of goethite containing Mn are more complex with the development of a distinct 'split' or endotherm doublet with increasing Mn content (Figure 3). Similar DTA patterns have been reported for Mn-bearing goethites produced under similar conditions and having undergone the same ammonium oxalate pretreatment (Stiers and Schwertmann, 1985). Consequently, the influence of ammonium oxalate towards the dehydroxylation behavior of goethite must, in this case, be considered as a possible cause of the DTA doublet (Figure 3). However, as development of the doublet increased with increasing Mn content, this also suggests an effect of Mn itself on the dehydroxylation behavior of goethite. This is discussed in more detail in later sections.

Dehydroxylation temperatures of goethites containing Ni and Ti were slightly greater than for the control goethites, but there was no significant trend with increasing Ni or Ti content (Figure 3). The larger Ti−O bond energy relative to the Fe−O bond (Table 2) has not resulted in an increase in the dehydroxylation temperature of Ti-bearing goethite. The smaller Ni−O bond energy relative to the Fe−O bond might be expected to reduce the temperature at which goethite dehydroxylates but effects of other changes in crystal composition associated with maintaining charge balance (*e.g.* incorporation of H^+ with Ni^{2+}, Carvalho-de-Silva *et al.*, 2003) may have acted to oppose this reduction.

The influence of crystal size and shape, particularly surface area (SA) on the temperature at which goethite dehydroxylates was tested by multiple linear regression analysis incorporating measurements of both SA and metal content (Table 4). Goethite containing Al and Mn were not included in the analysis because of the complex nature of their DTA patterns (*i.e.* multiple endotherms). Inclusion of SA significantly improved the prediction of endotherm temperature for goethite containing Cr, Ni and Ti as compared to the relationships between temperature and metal content alone (Table 4). Negative coefficients for SA for the Cr- and Ti-bearing goethites indicate that increasing SA tends to decrease endotherm temperature and partly offsets the increase in temperature associated with incorporation of Cr and Ti. However, partial F-tests of the relative significance of SA and metal content indicated Cr, Ni or Ti content as the most significant factor influencing endotherm temperature.

Thermal and XRD analysis of HCl-treated goethite

Examination of a control goethite (C1) and goethite containing 4.6 mol.% Al, 15.3 mol.% Mn and 12.2 mol.% Ti by XRD and DTA was conducted to investigate the reasons for the broad, multifaceted endotherms initially recorded for these oxalate-treated samples (Figure 3). These samples were all pretreated with 0.4 M HCl (refer to Methods section) prior to DTA and XRD analysis to avoid thermally induced effects associated with the decomposition of adsorbed ammonium oxalate-species as previously described.

The DTA patterns and weight-loss curves of HCl-treated, metal-bearing goethites (Figure 4) show: (1) a single broad endotherm over the temperature range 20−180ºC; (2) multiple or asymmetric endotherms over

Table 4. Multiple linear regression equations for goethite endotherm peak temperature (T) as a function of surface area (SA) and metal substitution.

Sample	Multiple regression	r^2	$r^{2\ \#}$
Cr	T = 282 + 3.58(mol.% Cr) − 0.393 (SA)	0.99**	0.99***
Ni	T = 249 + 3.09 (mol.% Ni) + 0.135 (SA)	0.95*	0.95***
Ti	T = 269 + 1.24 (mol.% Ti) − 0.201 (SA)	0.98*	0.63

Correlation coefficients for the simple, linear regression of endotherm temperature *vs.* metal content.
*** 99% confidence limit
** 95% confidence limit
* 90% confidence limit

https://doi.org/10.1346/CCMN.2006.0540204 Published online by Cambridge University Press

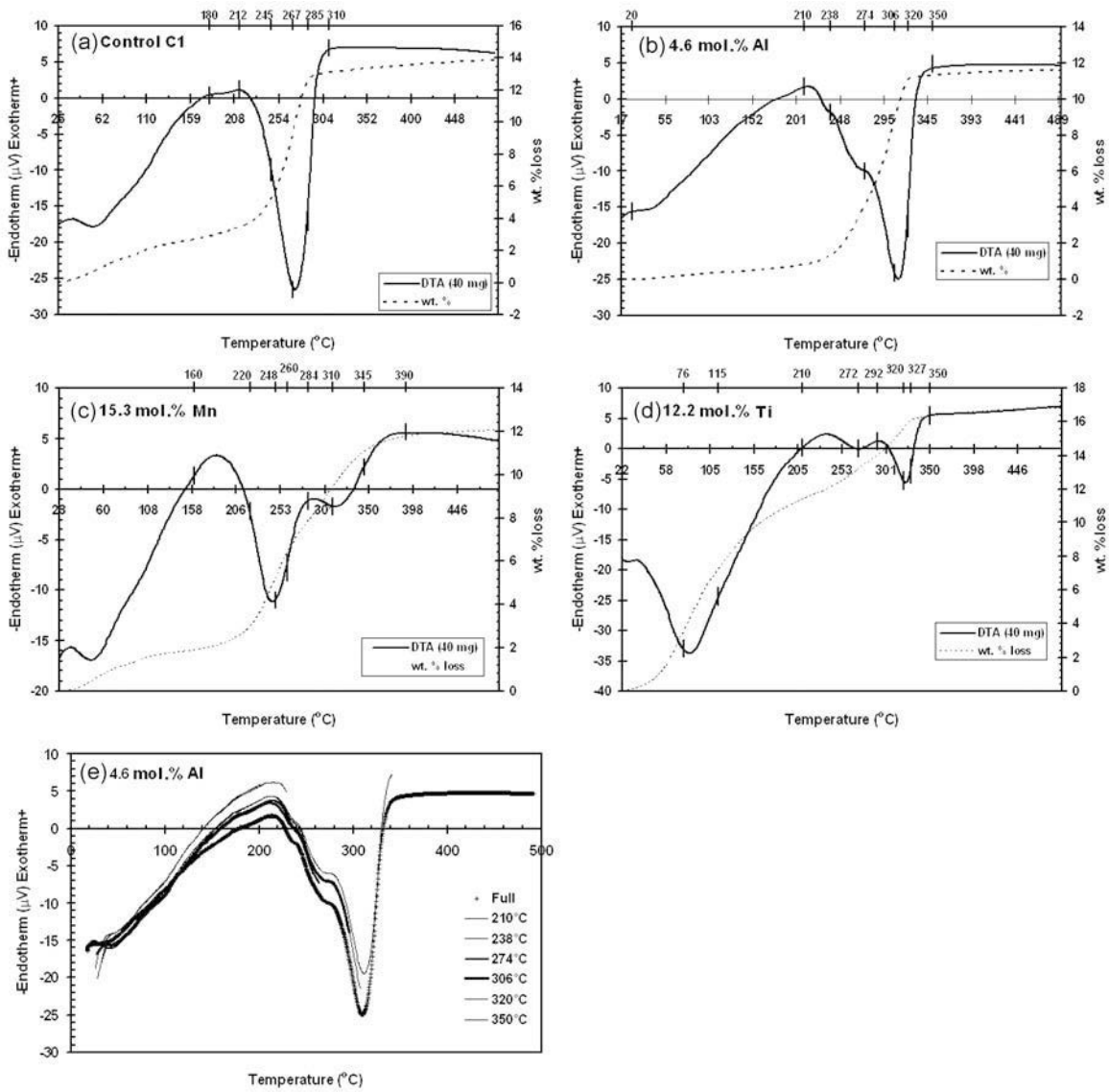

Figure 4. DTA patterns and weight loss (wt.%) curves for HCl-treated, control goethite (a), and for goethite containing 4.6 mol.% Al (b), 15.3 mol.% Mn (c) and 12.2 mol.% Ti (d). Positions marked on the DTA curve of each sample indicate the temperature to which fresh, individual 40 mg sub-samples were in each case heated for later XRD analysis. A composite plot of raw DTA data for individual sub-samples of HCl-treated goethite containing 4.6 mol.% Al, heated from ambient to the temperatures selected is given (e). The consistent and essentially identical thermal behavior observed for all HCl-treated samples (data not shown) demonstrates the homogeneous nature of the goethite samples examined.

the temperature range 200–350ºC (Figure 4). Heating to temperatures between 20 and 180ºC did not produce any detectable changes in unit-cell dimensions or changes in goethite unit-cell volume (Figure 5) despite the significant loss in weight recorded (Figure 4). Similar results were reported from the Rietveld refinement of synchrotron powder XRD (SXRD) during an investigation of the goethite-hematite phase transformation (Gualtieri and Venturelli, 1999). The small changes in unit-cell dimensions detected by heating from ambient to 200ºC were attributed to thermal expansion and structural relaxation effects (Gualtieri and Venturelli, 1999) in which detection was due to the very high quality of SXRD data collected, compared to the more conventional XRD analysis used in the present study.

For the synthetic goethite sample examined by Gualtieri and Venturelli (1999), refinement of the goethite H^+ population did not show any variation (*i.e.* loss in structural water content) nor was any decrease in crystallite size, preceding the transformation to hematite, detected by heating goethite to ~200ºC. In the present study, only small changes in mean crystallite dimensions (MCD) were determined, limited mainly to a decrease in MCD*c* values for the control (C1) and Al- and Mn-

https://doi.org/10.1346/CCMN.2006.0540204 Published online by Cambridge University Press

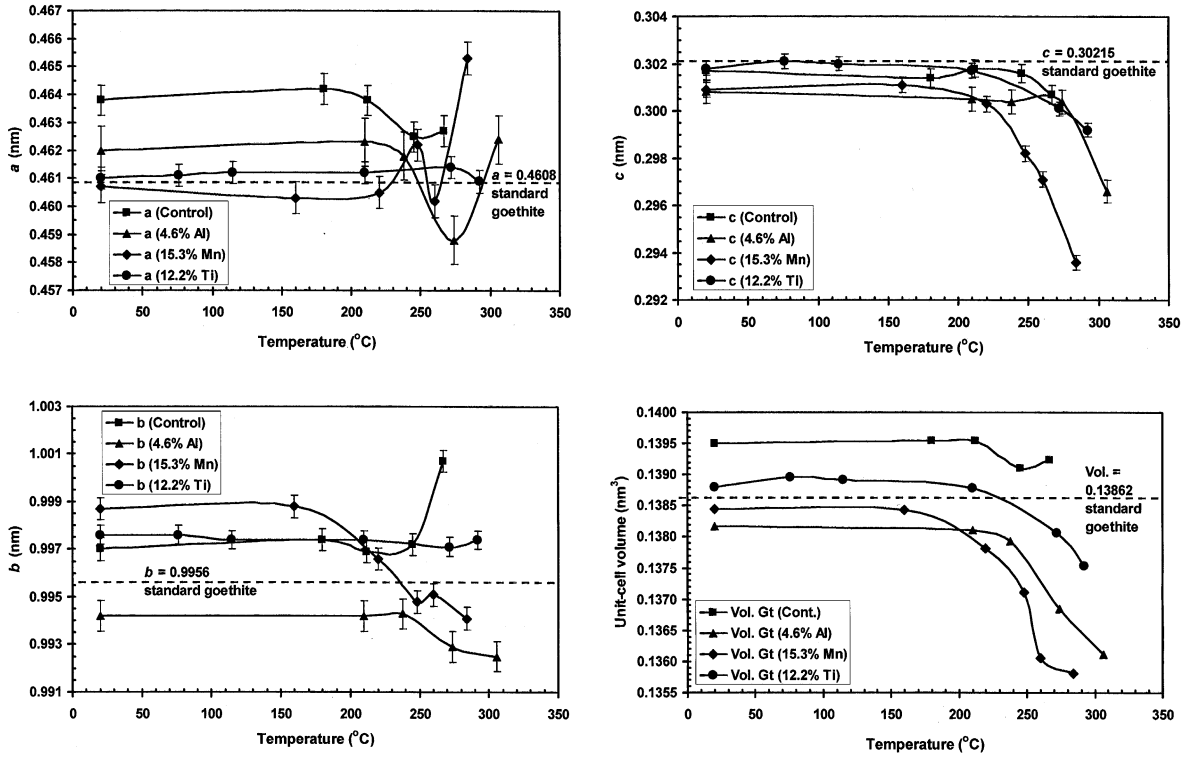

Figure 5. *a*, *b*, *c* and unit-cell volume determinations *vs.* temperature of HCl-treated control goethite and goethite containing 4.6 mol.% Al, 15.3 mol.% Mn and 12.2 mol.% Ti. Values of *a*, *b*, *c* and unit-cell volume are also plotted (dashed lines) for standard goethite, card 29-713 (JCPDS, 1986) for comparison.

bearing goethites (Figure 7). This apparent decrease may be a result of the limited number of goethite reflections used to determine crystallite size. Most MCD*c* values of goethite were averaged from only two to three reflections and may not be as reliable compared to values of MCD*a* and MCD*b*, determined by averaging crystallite sizes calculated from typically eight or nine goethite reflections.

Therefore, weight loss at temperatures <180ºC is not associated with any bulk structural changes in goethite, and probably represents loss of surface water as loosely bound and coordinated OH groups.

Endotherm formation at temperatures <100ºC has been reported for synthetic goethite and was attributed to surface-water desorption (Mackenzie and Berggren, 1970; Derie *et al.*, 1976; Schwertmann *et al.*, 1985). For control goethite and for goethite containing 4.6 mol.% Al and 15.3 mol.% Mn, desorption of surface water constituted a minor proportion (*i.e.* <0.2 or 20%) of the total weight loss recorded (Table 5). In contrast, goethite containing 12.2 mol.% Ti recorded a significant loss of surface water, which comprised ~60% of the total loss in weight observed (Table 5). This sample contained no X-ray amorphous constituents and consisted solely of large, blocky lath-shaped crystals. Cracks, fissures and intra-domain cavities are evident in the crystals of the Ti-bearing goethite (Figure 2), and this micro-porosity would account for the relatively large surface area (88 m^2/gm) recorded for this goethite (Table 1), and, hence, the high levels of surface water detected.

Table 5. Weight loss for HCl-treated, pure and metal-substituted goethite.

Sample	Wt.% loss			Weight loss as proportion of total wt.% loss	
	20−180ºC	180−500ºC	20−500ºC	20−180ºC[1]	180−500ºC[2]
Control (C1)	2.86	11.0	13.9	0.21	0.79
4.6 mol.% Al	0.80	11.1	11.7	0.05	0.95
15.3 mol.% Mn	2.02	10.0	12.1	0.17	0.83
12.2 mol.% Ti	10.6	6.18	16.8	0.63	0.37

[1] wt.% loss from 20−180ºC as a proportion of the total loss in weight by heating from 20º to 500ºC *e.g.* 0.21 = 2.86/13.9
[2] wt.% loss from 180−500ºC as a proportion of the total loss in weight by heating from 20º to 500ºC *e.g.* 0.79 = 11.0/13.9.

https://doi.org/10.1346/CCMN.2006.0540204 Published online by Cambridge University Press

The control goethite and goethite containing 4.6 mol.% Al both recorded a weight loss of 11% by heating from 180 to 500ºC, which is slightly greater than for standard goethite (10.1 wt.%), whereas the loss of 10.0 wt.% for the Mn-bearing goethite was the same as for standard goethite (Table 5). In contrast, the loss of 6.2 wt.% for goethite containing 12.2 mol.% Ti is significantly less than for standard goethite (Table 5). One explanation for this may be the presence of an associated anhydrous phase, such as hematite. In a binary system comprising only pure goethite and hematite, a 6 wt.% loss is equivalent to 40 wt.% hematite, an amount easily detected by XRD. However, no other phases were detected by XRD that would account for this reduced loss in weight. An alternative explanation may be in the nature of the substitution of Fe^{3+} by Ti^{4+}, and involve O^{2-} ions replacing OH^- in the goethite structure (*i.e.* loss of a proton). For example, the structural formula for the Ti-bearing goethite can be written as:

$$Fe^{3+}_{0.88}Ti^{4+}_{0.12}O^{2-}_{1.12}(OH^-)_{0.88}$$

This dehydroxylates, assuming the same molar Fe/Ti ratio in the resulting hematite, *via* the following reaction:

$$2[Fe^{3+}_{0.88}Ti^{4+}_{0.12}O^{2-}_{1.12}(OH^-)_{0.88}] \rightarrow Fe^{3+}_{1.76}Ti^{4+}_{0.24}O^{2-}_{3}(OH^-)_{0.24} + 0.76H_2O$$

with the measured loss in weight of 6.8% by heating from 180 to 500ºC, close to theoretical loss in weight of 7.6% for the above reaction. An even closer agreement between the predicted and measured (7.3 wt.%) loss in weight was observed by increasing the range in temperature (150–500ºC) for which weight loss was determined.

As will be discussed in more detail later, the recorded losses in weight for the HCl-treated control and metal-bearing goethite are associated with detectable and significant changes in the unit-cell parameters of goethite and of hematite formed from goethite. Bulk dehydroxylation of HCl-treated, metal-bearing goethite is characterized by a distinct endotherm doublet, which is particularly well developed for Mn- and Ti-bearing goethite, with the first endotherm occurring at 270ºC for goethite containing 4.6 mol.% Al and 12.2 mol.% Ti. This decreased to ~240ºC for goethite containing 15.3 mol.% Mn (Figure 4). This endotherm appears equivalent to that developed for HCl-treated control goethite C1 that occurs at 270ºC, with the small decrease in temperature observed for the Mn-bearing goethite probably due to the slightly smaller Mn–O/OH bond energy compared to that for Fe (Table 2).

Double dehydroxylation endotherm development

Previous DTA studies of the transformation of goethite to hematite have reported a 'split' or double endotherm for both natural and synthetic goethite (Derie *et al.*, 1976; Stiers and Schwertmann, 1985), although pre-treatment with ammonium oxalate complicates the results observed by Stiers and Schwertmann (1985). However, for untreated samples this phenomenon was explained in terms of the crystallinity of the precursor goethite. For poorly ordered goethite, with a = 4.63 Å ('high-a') or well-ordered goethite with a = 4.61 Å ('low-a'), transformation to hematite occurred at low and high temperatures, respectively, with only a single endotherm resulting in each case (Schwertmann, 1984; Schwertmann *et al.*, 1985). Heating of untreated material comprising a mixture of 'high-a' and 'low-a' goethite, with an intermediate a value of 4.62 Å, produces the endotherm doublet (Schwertmann, 1984; Schwertmann *et al.*, 1985). However, other factors such as sample preparation, sample size and the type of atmosphere during heating can also influence the shape of the endotherm (Mackenzie and Mitchell, 1970). For example, the adsorption of surface anions can influence both the shape and temperature at which goethite dehydroxylation occurs (Paterson and Swaffield, 1980; Mackenzie *et al.*, 1981). Detection of H_2O loss from surface OH groups by thermal analysis requires the rapid removal of evolved water vapour from goethite particles that are free of contaminant surface ions in samples with a high SA to particle volume (Mackenzie *et al.*, 1981). Consequently, detection of surface OH groups was reported only for small sample sizes of $\leqslant$10 mg (Mackenzie *et al.*, 1981). These effects are not detected in larger sample sizes (>~20–25 mg) presumably due to a 'swamping' effect caused by the bulk dehydroxylation of goethite.

Recently, Ford and Bertsch (1999) examined the origin of multiple thermal events using high-resolution, thermogravimetric analysis (HRTGA) of goethite prepared in the presence of small amounts (<2 mol.%) of Pb and/or Mn. Initial weight loss events were attributed to the decomposition of surface-coordinated OH-groups (=S_1OH, =S_2OH, =S_3OH) occurring at ~200–260ºC followed by bulk goethite dehydroxylation at ~270–280ºC. The results of Ford and Bertsch (1999) were obtained using only small samples sizes (5 mg), a condition which, according to Mackenzie *et al.* (1981), would maximize detection of small surface desorption effects. However, samples examined by Ford and Bertsch (1999) were also multi-mineralic comprising mixtures of hematite, ferrihydrite and goethite of two different morphologies (*e.g.* acicular crystals and multi-domainic laths), the dehydroxylation of which may have modified the form of the HRTGA curves observed.

Goethite phase transformation. Significant changes were detected in the unit-cell dimensions, unit-cell volume and, to a lesser extent, MCD values along the crystallographic axes of goethite and of hematite formed from goethite by heating from 180 to 350ºC. In addition, all four samples recorded a significant decrease in the

https://doi.org/10.1346/CCMN.2006.0540204 Published online by Cambridge University Press

goethite peak intensity ratio, Gt_{110}:Gt_{130}, caused by heating from 180 to 250ºC prior to development of the first, 'low-temperature' (low-*T*) endotherm. Changes in the Gt_{110}:Gt_{130} ratio were used to monitor the phase transformation of goethite and provide a relative indication of the formation of hematite as both the goethite 130 and hematite 104 reflections are coincident with a *d* value of 2.69 Å. A decrease in the Gt_{110}:Gt_{130} ratio and detection of the hematite 012 reflection at 3.67 Å revealed the presence of hematite prior to the development of the second, high-*T* endotherm occurring at ~310–320ºC for the metal-bearing goethites (Figure 4).

Changes in goethite *a* and *b* dimensions with heating from 180–300ºC were not consistent, whereas more consistent changes in values of *c* with heating were observed, with *c* decreasing significantly especially for goethite containing 4.6 mol.% Al and 15.3 mol.% Mn (Figure 5). This decrease was also reflected in a significant contraction in the goethite unit-cell volume due to heating from 180 to 350ºC (Figure 5). This is consistent with the marked decrease along *c* and overall decrease in cell volume for unsubstituted synthetic goethite before final conversion to hematite (Schwertmann *et al*., 1985; Gualtieri and Venturelli, 1999). The decrease was attributed to structural relaxation about vacancies resulting from proton migration during initial phase transformation of goethite to hematite (Gualtieri and Venturelli, 1999). The decrease in *c* and unit-cell volume of 2.43% and 1.89%, respectively, for goethite containing 15.3 mol.% Mn was the largest determined of the four goethite samples examined (Table 6).

On the basis of the percentage decrease in *c* and unit-cell volume on a per mol basis (% mol^{-1}), Al had the largest effect on *c* (*i.e.* 1.39%/4.6 mol.% = 0.31% mol.%$^{-1}$) and unit-cell volume (0.33% mol.%$^{-1}$) compared to Mn (*c* = 0.16% mol.%$^{-1}$; vol = 0.12% mol.%$^{-1}$) or Ti (*c* = 0.07% mol.%$^{-1}$; vol = 0.08% mol.%$^{-1}$). On this basis, the influence that metal ions have on *c* and the unit-cell volume of partially dehydroxylated goethite follows the sequence: Ti (low) < Mn < Al (high). Sequence order is not entirely related to ionic radius of the cation or *M*–O bond energy (Table 2), although the large effect of Al^{3+} on the contraction of the *c* dimension and unit volume is probably due to the significantly smaller size of the trivalent cation, which is some 17% smaller than Fe^{3+}, compared to either Mn^{3+} (same size as Fe^{3+}) or Ti^{4+} (6.2% smaller than Fe^{3+}). Other factors that may influence the sequence order include charge considerations for the tetravalent Ti ion, and the Jahn-Teller effect for Mn^{3+}.

According to the dehydroxylation model proposed by Schwertmann (1984) and Schwertmann *et al.* (1985), *a* values for untreated control goethite (C1) classify it as a 'high-*a*' type (*a* = 4.638 Å), goethite containing 4.6 mol.% Al as an intermediate type (*a* = 4.62 Å), whilst both the Mn- and Ti-bearing goethites would be described as 'low-*a*' types (*a* values of 4.607 Å and 4.601 Å, respectively). The DTA curves recorded for both the control and Al-bearing goethite are consistent with the dehydroxylation model proposed by Schwertmann (1984) and Schwertmann *et al*. (1985). However, multiple endotherm formation for the apparently 'low-*a*' Mn- and Ti-bearing goethite of this study is not consistent with this model, where only a single endotherm should be observed.

The conclusions of Schwertmann (1984) and Schwertmann *et al*. (1985) were based on the thermal examination of unsubstituted and Al-bearing goethite of variable crystallinity. In their work, the substitution of Fe^{3+} by metal cations with complex ionic properties, such as Mn^{3+} and Ti^{4+}, and their effect on the thermal behavior of goethite was not examined.

The HCl-treated control and metal-bearing goethites examined in the present study are, importantly in each case, morphologically uniform and mono-mineralic (Figure 2). Acid dissolution studies of these metal-substituted goethites showed that Al and Mn were uniformly incorporated, whereas Ti is concentrated towards the surface of goethite crystals (Wells, 1998). In the case of Mn, the long-range structural order of Mn-substituted goethite is retained for Mn contents in the range 0.13–0.18 (13–18 mol.%), whereas groutite-like clusters within the goethite structure develop at higher

Table 6. Unit-cell *c* dimension and volume of unheated and partially dehydroxylated HCl-treated control and metal-bearing goethite.

Sample	Unheated (*i.e.* 20ºC)		Heated (partially dehydroxylated)			% Change (decrease)	
	c (nm)	Vol. (nm^3)	*c* (nm)	Vol. (nm^3)	Temp. (ºC)	*c*[1]	Vol.[2]
Control C1	0.3017(4)	0.1395	0.3007(2)	0.1392	367	0.33	0.20
4.6 mol.% Al	0.3008(3)	0.1382	0.2966(7)	0.1361	306	1.39	1.47
15.3 mol.% Mn	0.3009(2)	0.1384	0.2936(9)	0.1358	284	2.43	1.89
12.2 mol.% Ti	0.3018(3)	0.1388	0.2992(4)	0.1375	292	0.86	0.91

[1] Percentage decrease in *c* of partially dehydroxylated goethite compared to *c* of unheated goethite *e.g.* 0.33 % = (0.3017–0.3007)/0.3017 × 100%.
[2] Percentage decrease in unit-cell volume of partially dehydroxylated goethite compared to the unit-cell volume of unheated goethite, *e.g.* 0.20% = (0.1395–0.1392)/0.1395 × 100%.

https://doi.org/10.1346/CCMN.2006.0540204 Published online by Cambridge University Press

Mn contents (Scheinost *et al.*, 2001). In this study, the maximum substitution of 15 mol.% Mn in goethite occurs towards the lower end of this transition range so that groutite-like clustering of Mn within goethite is unlikely to occur. Indeed, Scheinost *et al.* (2001) suggested that the probability of groutite-like clusters forming within goethite at a Mn content of 0.2 (*i.e.* 20 mol.%) would still be very low. Therefore, multiple DTA events recorded for goethite containing 15.3 mol.% Mn are not the result of the dehydroxylation of populations of goethite particles of different size and shape or related to localized concentrations of Mn within goethite.

Morphologically, HCl-treated goethite containing 12.2 mol.% Ti appears texturally uniform (Figure 2) so that the complex thermal behavior recorded may be associated with surface concentrations of Ti (Wells, 1998). In addition, the influence of Ti on the local structure around Fe is unknown and requires further study using X-ray spectroscopic techniques (*e.g.* EXAFS). However, an examination can still be made of bulk structural effects associated with the incorporation of Ti and its influence during the thermal transformation of goethite to hematite.

Unit-cell parameters of newly formed hematite. Despite the error in determinations of *a* and *c* unit-cell dimensions and, in particular, the unit-cell volume of hematite formed by the dehydroxylation of goethite generally decreased with heating from 300 to 500ºC (Figure 6). In all cases the unit-cell volume of hematite first formed by the dehydroxylation of goethite was up to 1.17% larger than that for hematite heated at 500ºC (Table 7). This trend is consistent with the reportedly larger size of the unit-cell volume for hematite first formed by the dehydroxylation of goethite compared to well ordered hematite formed at higher temperatures (Brown, 1980).

Trends in the variation of *a*, *c* and values of unit-cell volume of hematite with heating from 300 to 500ºC were not related to whether an endotherm doublet was observed or not. Hence, formation of the second, high-*T* endotherm does not appear related to changes in the unit-cell parameters of hematite.

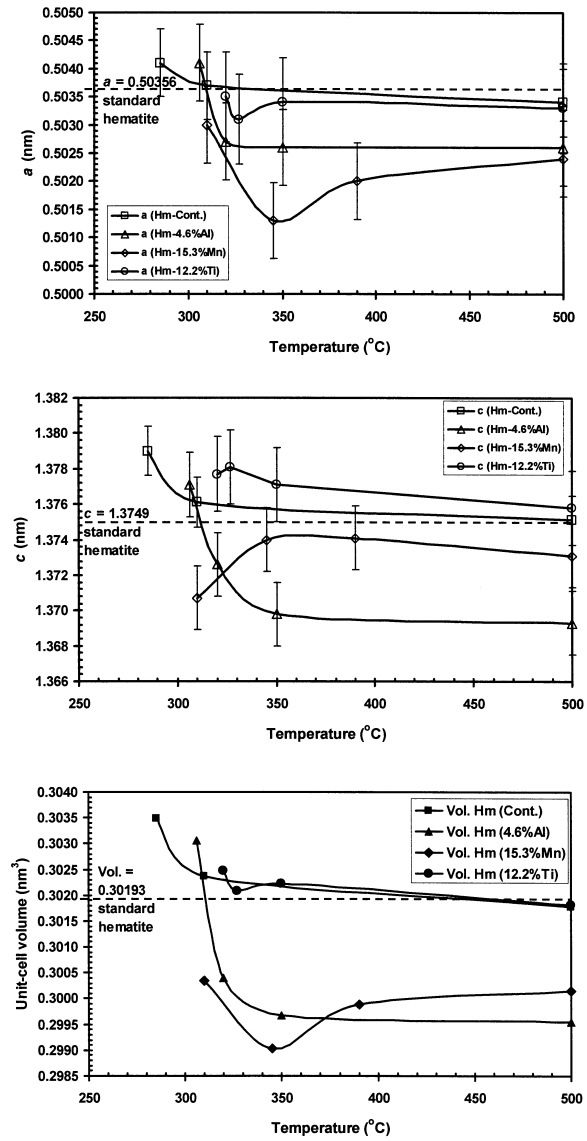

Figure 6. *a*,*c* and unit-cell volume determinations *vs.* temperature of hematite produced by heating HCl-treated control goethite and goethite containing 4.6 mol.% Al, 15.3 mol.% Mn and 12.2 mol.% Ti. Values of *a*, *c* and unit-cell volume are also plotted (dashed lines) for standard hematite, starred card 33-664 (JCPDS, 1986) for comparison.

Table 7. Unit-cell volume of hematite initially transformed from goethite and heated at 500ºC.

Sample	Hematite unit-cell volume (nm^3) Newly formed	500ºC	% Change (increase)[2]
Control C1	0.3035 (285ºC)[1]	0.3018	0.56
4.6 mol.% Al	0.3031 (306ºC)	0.2996	1.17
15.3 mol.% Mn	0.3003 (310ºC)	0.3002	0.06
12.2 mol.% Ti	0.3025 (320ºC)	0.3018	0.22

[1] Temperature, in parentheses, of hematite formation.
[2] Percentage increase in unit-cell volume of newly formed hematite compared to the unit-cell volume of hematite formed from goethite heated at 500ºC *e.g.* 0.56% = (0.3035−0.3018)/0.3018 × 100%.

https://doi.org/10.1346/CCMN.2006.0540204 Published online by Cambridge University Press

Mean crystallite dimensions along the *a* and *c* axes of hematite initially formed from goethite show a rapid, up to two-fold increase over the temperature range 300–350ºC, followed by a decelerating increase with heating to 500ºC (Figure 7). Despite the increase in MCD values, which may occur through a mechanism of domain coalescence or recrystallization, significant line broadening was still observed in XRD patterns. Considering the crystallographic orientation of goethite and hematite where the *a* and *c* directions of goethite becomes the *c* and *a* directions, respectively, of hematite (Francombe and Rooksby, 1959), at transformation, the hematite structure along the *a* axis is fully developed whereas structural ordering along the hematite *c* direction is only fully developed with heating at higher temperatures (>700ºC) (Francombe and Rooksby, 1959; Brown, 1980). Structural refinement of the octahedral site Fe population in newly formed hematite demonstrated the presence of a disordered Fe distribution as a faulted, planar stacking sequence along *c* (Gualtieri and Venturelli, 1999). This is manifested in XRD patterns as a preferential or anisotropic line broadening of hematite $h + k = 3n$ and $l \neq 3n$ (*e.g.* 012, 104 and 204) reflections compared to reflections where $l = 3n$ (*e.g.* 110, 113 and 116). Values of the WHH (width at half height) ratio for the hematite 104 and 110 reflections, WHH104:WHH110,

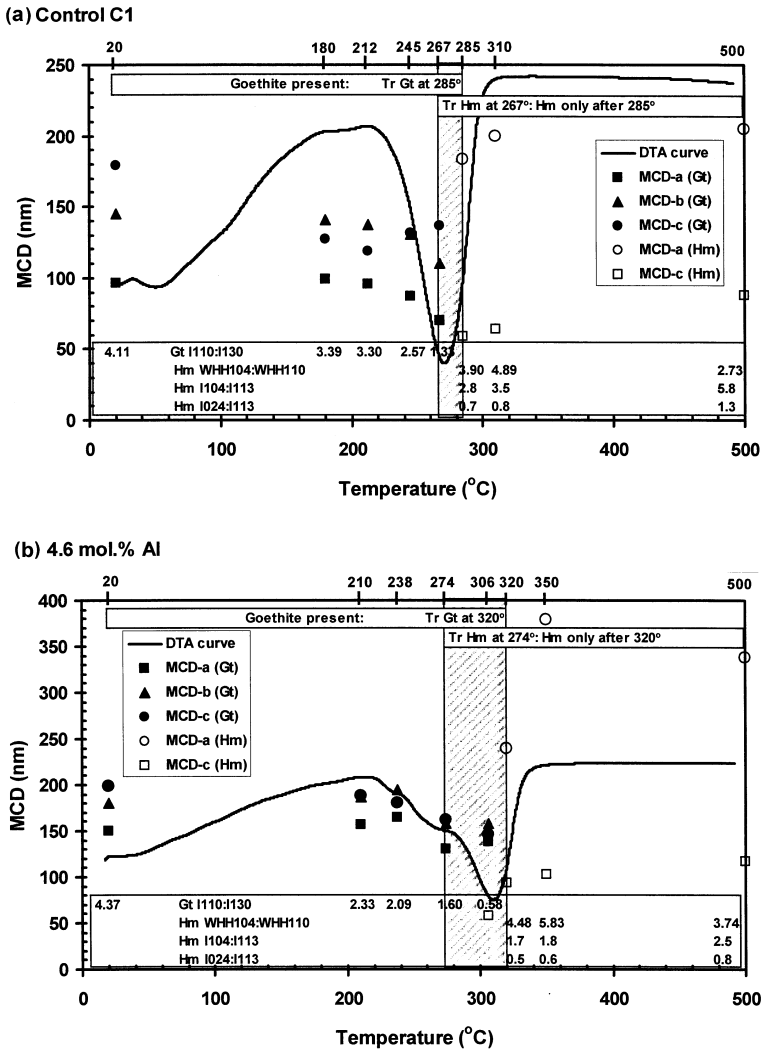

Figure 7 (*this and facing page*). Mean crystallite dimensions (MCD) along the *a*, *b* and *c* directions (MCD*a*, MCD*b* and MCD*c*, respectively) of HCl-treated (a) control goethite and goethite containing (b) 4.6 mol.% Al, (c) 15.3 mol.% Mn and (d) 12.2 mol.% Ti, and values of MCD*a* and MCD*c* for hematite obtained by the dehydroxylation of the precursor control and metal-bearing goethite *vs.* temperature. The hematite MCD*a* value at 327ºC in (d) (starred), was not corrected for instrumental broadening. DTA curves are presented as an overlay for comparative purposes. The shaded box in each case represents the range in temperature over which hematite was first detected to the temperature at which goethite vanished. Values of XRD pattern peak ratios for goethite (Gt I110:I130) and newly formed hematite (Hm WHH104:WHH110, Hm I104:I113, HmI024:I113) are presented in the inset box for each sample. Refer to the text for an explanation of these ratios.

https://doi.org/10.1346/CCMN.2006.0540204 Published online by Cambridge University Press

used as a measure of line broadening for hematite formed from the control goethite (C1) and the Al-, Mn- and Ti-bearing goethites, are markedly greater than unity as would be the case for well-ordered hematite with no anisotropic peak broadening (Figure 7). Thus, ordering of the hematite structure along the *c* direction for these samples is not fully developed by heating at 500ºC.

Significant losses in weight of 7.33 wt.% (interval 274–350ºC), 3.53 wt.% (284–390ºC) and 2.28 wt.% (292–350ºC) were recorded for the Al-, Mn- and Ti-bearing goethites, respectively. These weight losses account for ~65, 35 and 37% of the total weight loss recorded by heating the Al-, Mn- and Ti-bearing goethites, respectively, from 180 to 500ºC. Still significant losses in weight of 0.31 wt.% (350–500ºC, Al), 0.32 wt.% (390–500ºC, Mn) and 0.45 wt.% (350–500ºC, Ti) were recorded at temperatures at which hematite was the only phase detected by XRD.

Hematite first formed by the dehydroxylation of goethite can retain up to half the stoichiometric water content of the parent goethite, with OH^- replacing O^{2-} ions resulting in a non-stoichiometric hematite (Wolska and Schwertmann, 1989). Structural refinement, using synchrotron powder XRD data, of the Fe, H and O populations in the phase first formed by the transformation of goethite confirmed the occurrence of the non-stoichiometric or protohematite phase (Gualtieri and Venturelli, 1999), with a composition very close to that postulated by Wolska and Schwertmann (1989). Phase characterization demonstrated the persistence of OH groups to 800ºC wherein protohematite fully transformed to hematite proper (Gualtieri and Venturelli, 1999). Thus, the protohematite phase described by Gualtieri and Venturelli (1999) may then be used to include phases previously described as protohematite and hydrohematite (Figure 1).

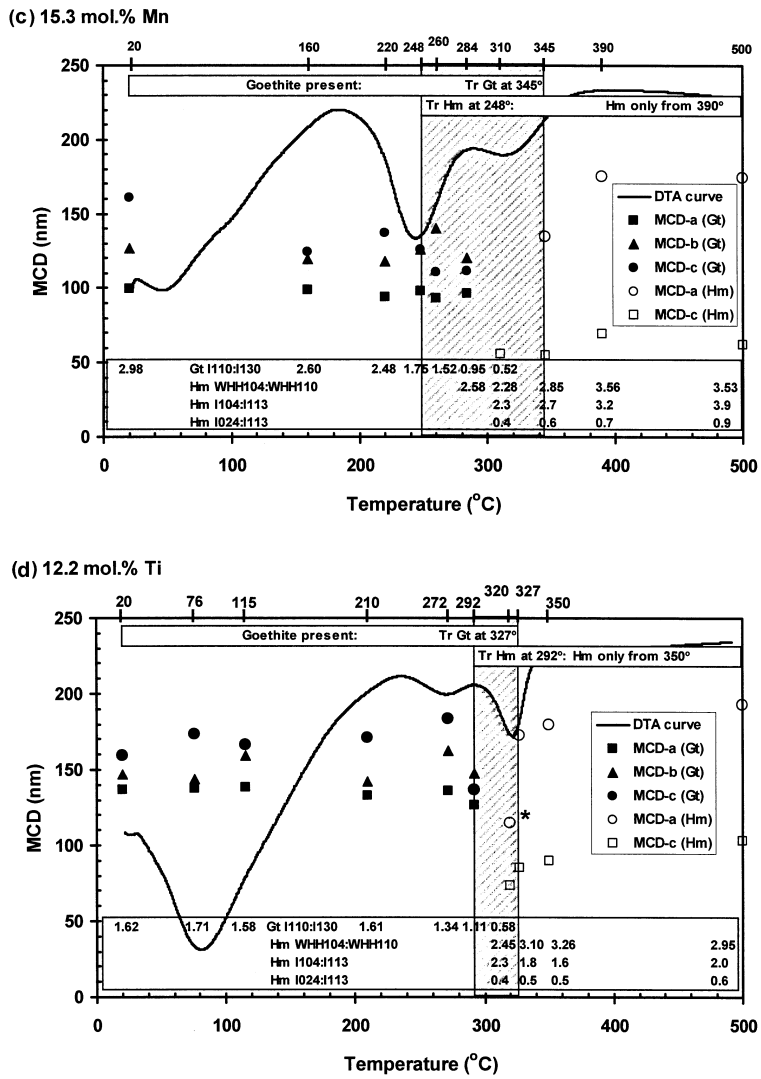

Figure 7 (*contd.*).

https://doi.org/10.1346/CCMN.2006.0540204 Published online by Cambridge University Press

The presence of OH in protohematite results in an Fe deficiency in the cationic sub-structure, which can be detected by a reduction in the intensity of the I_{hkl}/I_{113} ratio for the 012, 104, 110 and 024 peaks. In particular, the I_{104}/I_{113} and I_{024}/I_{113} ratios are the most sensitive to incorporated OH groups in the hematite structure (Wolska and Schwertmann, 1989). The intensity of the 113 reflection relates only to the oxygen anionic sub-structure and so is not affected by a deficiency in Fe (Wolska and Schwertmann, 1989).

Values of I_{104}/I_{113} and I_{024}/I_{113} for hematite, obtained by the dehydroxylation of Al-, Mn- and Ti-bearing goethite, were significantly less than the theoretical values of 5 and 2 for I_{104}/I_{113} and I_{024}/I_{113}, respectively, of well crystallized (*i.e.* OH-free) hematite (Figure 7). This confirms that protohematite was produced *via* the dehydroxylation of goethite containing Al, Mn and Ti for temperatures up to 500ºC. The exception is for the phase formed from control goethite, where values for I_{104}/I_{113} and I_{024}/I_{113} at 500ºC approached those of standard, OH-free hematite (Figure 7), indicating the formation of hematite, *sensu stricto*, in this case.

The rapid increase in MCD*a* and MCD*c* for protohematite formed from Al-, Mn- and Ti-bearing goethite, coincidental with development of the second, high-*T* endotherm recorded for these samples, is associated with the loss of significant amounts of water. Simple domain growth and structural (*i.e.* unit-cell) changes of protohematite during transformation would probably produce an exothermic effect so that the second, high-*T* endotherm is probably due to the evolution of OH during hematite domain growth combined, in part, with water loss from residual goethite.

This model is entirely consistent with the observations by Goss (1987), later confirmed by Gualtieri and Venturelli (1999) concerning the phase transformation of goethite. Goss (1987) demonstrated that goethite dehydroxylation starts at the surface of goethite particles and proceeds inwards with the formation of empty layers (pores) parallel to the *b*-*c* plane of goethite (space group *Pbnm*). This is consistent with the long-range diffusion of OH^- and H^+ along channels parallel to the *c* direction, which results in the first endotherm (Gualtieri and Venturelli, 1999). Formation of the second endotherm was then due to condensation of H_2O and expulsion from the reacting goethite as a consequence of OH migration along *c* and the redistribution of Fe within protohematite (Gualtieri and Venturelli, 1999).

However, it is at this point where the model of Gualtieri and Venturelli (1999) is not consistent with observations of the present study. Initial diffusion of OH^- and H^+ along cavities along the *c* direction that resulted in the first endotherm was considered only significant in large particles, and the larger the grain size the larger the area of the first peak (Gualtieri and Venturelli, 1999). A comparison of particle size for Al-, Mn- and Ti-bearing goethite (Figure 2) shows the opposite effect, particularly for Ti-substituted goethite where the area of the first endotherm appears much smaller than the area of the second (Figure 4). The model of Gualtieri and Venturelli (1999) is based on characterizing the phase transformation of only a single, unsubstituted synthetic goethite where the influence of incorporated metal cations on the thermal behavior of goethite was not examined. In addition, changes in the crystallite size of protohematite with heating were not described by Gualtieri and Venturelli (1999).

The extent of domain growth during and immediately following the transformation of goethite to hematite would be influenced, *inter alia*, by the presence of metal ion impurities (Al, Mn and Ti) within hematite. No other discrete phases were detected, to the limit of detection of ~2 wt.%, in XRD patterns of hematite formed at 500ºC from the precursive, metal-bearing goethite. Therefore, it was assumed that Al, Mn and Ti initially present in the parent goethite were retained in the transformed hematite structure and did not form discrete oxides or other compounds. This is a reasonable assumption given that structural ordering of protohematite heated at temperatures up to 500ºC is not fully developed and so may easily accommodate metal cations.

The presence of Al, Mn and Ti may affect goethite transformation to hematite and subsequent domain growth by local distortion of the protohematite structure in regions immediately surrounding the metal cation that inhibits or delays recrystallization causing it to occur at higher temperatures. Qualitative evidence for this is shown in the increase of the range in temperature over which hematite was first detected to the temperature at which goethite ceased to persist (Figure 7) with incorporation of Al, Mn and Ti. This temperature range (ΔT_{Gt+Hm}) was only 20ºC for the control goethite, whereas ΔT_{Gt+Hm} increased markedly with incorporation of 4.6 mol.% of Al (ΔT_{Gt+Hm} ~50ºC), 15.3 mol.% Mn (ΔT_{Gt+Hm} ~100ºC) and 12.2 mol.% Ti (ΔT_{Gt+Hm} ~35–40ºC) (Figure 7). It is not unwarranted to consider that for the elements examined in the present study, the inhibitory effect of each cation would be different in each case due to differences in the ionic properties of each cation. Whilst Mn and Ti were incorporated at similar levels within goethite (*e.g.* 15.3 *vs.* 12.2 mol.%, respectively), the DTA curves for each goethite were very different (Figure 4). Not only is the initial distribution of Mn and Ti within the precursor goethite important, but effects arising from the incorporation of octahedrally distorted Mn^{3+} (Jahn-Teller effect) or tetravalent Ti, would also be important.

It appears that during heating of Al-, Mn- and Ti-bearing goethite, initial dehydroxylation occurs with the formation of some protohematite, until a point is reached where the rate of transformation (and weight loss) decreases, and domain growth of protohematite slows. This produces the first, 'low-*T*' endotherm. Transformation of unsubstituted goethite is not inhibited

https://doi.org/10.1346/CCMN.2006.0540204 Published online by Cambridge University Press

and the growth of protohematite domains along *a* and *c* directions occurs spontaneously with continuous evolution of OH^- resulting in only a single dehydroxylation event. With continued heating of the metal-bearing goethite, a critical temperature is reached, modified by the foreign cation present that provides enough thermal energy to enable the transformation of goethite to proceed to completion. Evolution of water from residual goethite in conjunction with the loss of OH from protohematite, associated with the rapid growth in hematite crystallite size along *a*, produces the second, 'high-*T*' endotherm. Even though development of the hematite structure along *c* is less well developed than along *a*, thus giving rise to the anisotropic peak broadening effect, domain growth occurs mainly along the *a* direction of hematite. Formation of the endotherm doublet represents the evolution of the bulk of the water content in the system. However, small but detectable amounts of water remain in hematite following transformation, which is (presumably) gradually lost with heating to higher temperatures (*i.e.* >500ºC).

CONCLUSIONS

Combined XRD and thermal analysis of synthetic Al-, Cr-, Mn-, Ni- and Ti-bearing goethite has confirmed and extended the findings of previous research that examined thermal phenomena, such as development of an endotherm doublet, during the phase transformation of goethite to hematite. The thermal behavior that results is due to a combination of the nature of the precursor goethite (*i.e.* crystallinity) and how factors such as goethite chemistry influence the reaction kinetics (*i.e.* domain growth) of protohematite along the *a* and *c* directions before final conversion to hematite.

One aspect not examined in the present study, but requiring further investigation, is the nature of the transfer, retention and resulting distribution of metal cations from the parent goethite to hematite during transformation. Phase characterization using refinement of 'real-time' powder XRD, similar to the approach as used by Gualtieri and Venturelli (1999), in conjunction with TEM analysis to examine the influence of factors such as particle size and, in particular, particle shape is needed to describe fully the mechanisms of the thermal reaction.

ACKNOWLEDGMENTS

The authors thank the two reviewers for their comments, which greatly improved the manuscript. Kristy Blyth and Ian Sills of the Thermal Characterization Laboratory, Curtin University of Technology, Western Australia, are thanked for their assistance with the DTA analysis of HCl-treated goethite, and appreciation is extended to Phillipa Butterworth, CSIRO Land and Water, for performing the SA determinations of oxalate-treated samples. This work formed part of a study undertaken to complete PhD research by the first author (MAW) at the School of Earth and Geophysical Sciences, University of Western Australia.

REFERENCES

Anand, R.R. and Gilkes, R.J. (1987) The association of maghemite and corundum in Darling Range laterites, Western Australia. *Australian Journal of Soil Research*, **25**, 303–311.

Bernal, J.D., Dasgupta, D.R. and Mackay, A.L. (1959) The oxides and hydroxides of iron and their structural interrelationships. *Clay Minerals Bulletin*, **4**, 15–30.

Brown, G. (1980) Associated minerals. Pp. 361–410 in: *Crystal Structures of Clay Minerals and their X-ray Identification* (G.W. Brindley and G. Brown, editors). Monograph **5**, Mineralogical Society, London.

Burns, R.G. (1970) *Mineralogical Applications of Crystal Field Theory*. Cambridge University Press, London, 1st edition.

Carvalho-de-Silva, M.L., Ramos, A.Y., Tolentino, H.C.N., Enweiler, J., Netto, S.M. and Alves, M.C.M. (2003) Incorporation of Ni into natural goethite: An investigation by X-ray absorption spectroscopy. *American Mineralogist*, **88**, 876–882.

Cornell, R.M. and Schneider, W. (1989) Formation of goethite from ferrihydrite at physiological pH under the influence of cysteine. *Polyhedron*, **8**, 149–155.

Cornell, R.M., Giovanoli, R. and Schneider, W. (1992) The effect of nickel on the conversion of amorphous iron (III) hydroxide into more crystalline iron oxides in alkaline media. *Journal of Chemistry and Technical Biotechnology*, **53**, 73–79.

Cornell, R.M., Mann, S. and Skarnulis, A.J. (1983) A high resolution electron microscopy examination of domain boundaries in crystals of synthetic goethite. *Journal of the Chemical Society – Faraday Transactions*, **1**, 2679–2684.

Derie, R., Ghodsi, M. and Calvo-Roche, C. (1976) DTA study of the dehydration of synthetic goethite α-FeOOH. *Journal of Thermal Analysis*, **9**, 435–440.

Fitzpatrick, R.W. and Chittleborough, D.J. (2002) Titanium and zirconium minerals. Pp. 667–690 in: *Soil Mineralogy with Environmental Applications* (J.B. Dixon and D.G. Schulze, editors). SSSA Book Series No 7, Soil Science Society of America, Madison, Wisconsin.

Fitzpatrick, R.W., LeRoux, J. and Schwertmann, U. (1978) Amorphous and crystalline titanium and iron-titanium oxides in synthetic preparations, at near ambient conditions, and in soil clays. *Clays and Clay Minerals*, **26**, 189–201.

Ford, R.G. and Bertsch, P.M. (1999) Distinguishing between surface and bulk dehydration-dehydroxylation reactions in synthetic goethites by high-resolution thermogravimetric analysis. *Clays and Clay Minerals*, **47**, 329–337.

Francombe, M.H. and Rooksby, H.P. (1959) Structure transformations affected by the dehydration of diaspore, goethite and delta ferric oxide. *Clay Minerals Bulletin*, **4**, 1–14.

Gasser, U.G., Jeanroy, E., Mustin, C., Barres, O., Nuesch, R., Berthelin, J. and Herbillon, A.J. (1996) Properties of synthetic goethites with Co for Fe substitution. *Clay Minerals*, **22**, 31–39.

Goss, C.J. (1987) The kinetics and reaction mechanism of the goethite to hematite transformation. *Mineralogical Magazine*, **51**, 437–451.

Gualtieri, A.F. and Venturelli, P. (1999) In situ study of the goethite-hematite phase transformation by real time synchrotron powder diffraction. *American Mineralogist*, **84**, 895–904.

Handbook of Chemistry and Physics (1988) Table 1. Bond strengths in diatomic molecules. R. Weast (editor), CRC Press Inc., Florida.

Hsu, P.H. (1989) Aluminum hydroxides and oxyhydroxides. Pp. 99–143 in: *Minerals in Soil Environments* (J.B. Dixon and S.B. Weed editors). Soil Science Society of America, Madison, Wisconsin.

Huynh, T., Tong, A.R., Singh, B. and Kennedy, B.J. (2003) Cd-substituted goethites – a structural investigation by synchrotron X-ray diffraction. *Clays and Clay Minerals*, **51**, 397–402.

JCPDS (1988) *Mineral Powder Diffraction File, Data Book*. International Centre for Diffraction Data, Joint Committee on Powder Diffraction Standards, JCPDS, Pennsylvania, USA.

Klug, H.P. and Alexander, L.E. (1974) *X-ray Diffraction Procedures for Polycrystalline and Amorphous Materials*. John Wiley and Sons, New York, 996 pp.

Mackenzie, R.C. and Berggren, G. (1970) Oxides and oxyhydroxides of higher valency elements. Pp. 272–302: *Differential Thermal Analysis* (R.C. Mackenzie editor). Academic Press, London.

Mackenzie, R.C. and Mitchell, B.D. (1970) Technique. Pp. 101–122 in: *Differential Thermal Analysis* (R.C. Makenzie, editor). Academic Press, London.

Mackenzie, R.C., Paterson, E. and Swaffield, R. (1981) Observation of surface characteristics by DSC and DTA. *Journal of Thermal Analysis*, **22**, 269–274.

Manceau, A., Schlegel, M.L., Musso, M., Sole, V.A., Gauthier, C., Petit, P.E. and Trolard, F. (2000) Crystal chemistry of trace elements in natural and synthetic goethite. *Geochimica et Cosmochimica Acta*, **64**, 3643–3661.

Morris, R.V. and Lauer, Jr. H.V. (1981) Stability of goethite (α-FeOOH) and lepidocrocite (γ-FeOOH) to dehydration by UV radiation: Implications for their occurrence on the Martian surface. *Journal of Geophysical Research*, **86**, 10893–10899.

Naono, H. and Fujiwara, R. (1980) Micropore formation due to thermal decomposition of acicular microcrystals of α-FeOOH. *Journal of Colloid and Interface Science*, **73**, 406–415.

Novak, G.A. and Colville, A.A. (1989) A practical interactive least squares cell-parameter program using an electronic spreadsheet and a personal computer. *American Mineralogist*, **74**, 488–490.

Özdemir, Ö. and Dunlop, D.J. (2000) Intermediate magnetite formation during dehydration of goethite. *Earth and Planetary Science Letters*, **177**, 59–67.

Parfitt, R.L. (1989) Optimum conditions for extraction of Al, Fe and Si from soils with acid oxalate. *Communications in Soil Science and Plant Analysis*, **20**, 801–816.

Parfitt, R.L., Farmer, V.C. and Russell, J.D. (1977) Adsorption on hydrous oxides. I. Oxalate and benzoate on goethite. *Journal of Soil Science*, **28**, 29–39.

Paterson, E. and Swaffield, R. (1980) Influence of adsorbed anions on the dehydroxylation of synthetic goethite. *Journal of Thermal Analysis*, **18**, 161–167.

Ruan, H.D. and Gilkes, R.J. (1995) Dehydroxylation of aluminous goethite: Unit cell dimensions, crystal size and surface area. *Clays and Clay Minerals*, **43**, 196–211.

Scheinost, A.C., Stanjek, H., Schulze, D.G., Gasser, U. and Sparks, D.L. (2001) Structural environment and oxidation state of Mn in goethite-groutite solid-solutions. *American Mineralogist*, **86**, 139–146.

Schulze, D.G. and Schwertmann, U. (1984) The influence of aluminium on iron oxides. X. Properties of Al-substituted goethite. *Clay Minerals*, **19**, 521–539.

Schulze, D.G. and Schwertmann, U. (1987) The influence of aluminium on iron oxides. XIII. Properties of goethites synthesized in 0.3 M KOH at 25ºC. *Clay Minerals*, **22**, 83–92.

Schwertmann, U. (1984) The double dehydroxylation peak of goethite. *Thermochimica Acta*, **78**, 39–46.

Schwertmann, U. and Cornell, R.M. (1991) *Iron Oxides in the Laboratory*. VCH Publishing, Weinheim, Germany, 137 pp.

Schwertmann, U. and Pfab, G. (1994) Structural vanadium in synthetic goethite. *Geochimica et Cosmochimica Acta*, **58**, 4349–4352.

Schwertmann, U. and Taylor, R.M. (1989) Iron Oxides. Pp. 379–438 in: *Minerals in Soil Environments* (J.B. Dixon and S.B. Weed, editors). Soil Science Society of America, Madison Wisconsin, USA.

Schwertmann, U., Cambier, P. and Murad, E. (1985) Properties of goethites of varying crystallinity. *Clays and Clay Minerals*, **33**, 369–378.

Schwertmann, U., Gasser, U. and Sticher, H. (1989) Chromium-for-Fe substitution in synthetic goethites. *Geochimica et Cosmochimica Acta*, **53**, 1293–1297.

Shannon, R.D. (1976) Revised effective ionic radii and systematic studies of inter-atomic distances in halides and chalcogenides. *Acta Crystallographica*, **A32**, 751–767.

Singh, B. and Gilkes, R.J. (1992) Properties and distribution of iron oxides and their association with minor elements in the soils of south-western Australia. *Journal of Soil Science*, **43**, 77–93.

Smith, K.L. and Eggleton, R.A. (1983) Microstructures of botryoidal goethites. *Clays and Clay Minerals*, **31**, 392–396.

Stiers, W. and Schwertmann, U. (1985) Evidence for manganese substitution in synthetic goethite. *Geochimica et Cosmochimica Acta*, **49**, 1909–1911.

Suter, D., Banwart, S. and Stumm, W. (1991) Dissolution of hydrous iron(III) oxides by reductive mechanisms. *Langmuir*, **7**, 809–813.

Tessens, E. and Zauyah, S. (1982) Positive permanent charge in Oxisols. *Soil Science Society of America Journal*, **46**, 1103–1106.

Trolard, F., Bourrie, G., Jeanroy, E., Herbillon, A.J. and Martin, H. (1995) Trace metals in natural iron oxides from laterites: A study using selective kinetic extraction. *Geochimica et Cosmochimica Acta*, **59**, 1285–1297.

van Oosterhout, G.W. and Rooijmans, C.J.M. (1958) A new superstructure in gamma ferric oxide. *Nature*, **181**, 44–45.

Vempati, R.K., Morris, R.V., Lauer, H.V. Jr. and DeHart, J. (1991) Synthesis and properties of Ti-substituted goethites and hematites. *28th Annual Clay Minerals Society, Houston, Texas*.

Watari, F., Delavignette, P., Van Lunduyt, J. and Amelinckx, S. (1983) Electron microscopic study of dehydration transformations: The formation of 'superstructures' on the dehydration of goethite and diaspore. *Journal of Solid State Chemistry*, **29**, 417–427.

Weissenborn, P.K., Dunn, J.G. and Warren, L.J. (1994) Quantitative thermogravimetric analysis of haematite, goethite and kaolinite in Western Australian iron ores. *Thermochimica Acta*, **239**, 147–156.

Wells, M.A. (1998) Mineral, chemical and magnetic properties of synthetic, metal-substituted goethite and hematite. PhD thesis, University of Western Australia, 401 pp.

Wolska, E. and Schwertmann, U. (1989) Nonstoichiometric structures during dehydroxylation of goethite. *Zeitschrift für Kristallographie*, **189**, 223–237.

Wolska, E. and Szajda, W. (1985) Structural and spectroscopic characteristics of synthetic hydrohematite. *Journal of Materials Science*, **20**, 4407–4412.

(*Received 4 March 2005; revised 11 September 2005; Ms. 1021; A.E. Helge Stanjek*)